Engineering Analysis with Boundary Elements 156 (2023) 519–536

Contents lists available at ScienceDirect

Engineering Analysis with Boundary Elements

journal homepage: www.elsevier.com/locate/enganabound

An adaptive and efficient affine transformation-based subdivision method for evaluation of nearly singular integrals

Baotao Chi [a,b], Fushun Wang [a], Qianjian Guo [a,*], Yaoming Zhang [c], Chuanming Ju [d], Wei Yuan [a]

[a] School of Mechanical Engineering, Shandong University of Technology, Zibo 255000, China
[b] Shandong Luoxiang Automobile Manufacturing Postdoctoral Research Institute, Linyi 276211, China
[c] School of Mathematics and Statistics, Shandong University of Technology, Zibo 255000, China
[d] School of Electromechanical and Automotive Engineering, Yantai University, Yantai 264005, China

ARTICLE INFO

Keywords:
Boundary element method
Nearly singular integrals
Adaptive subdivision scheme
Affine transformation
Gaussian quadrature

ABSTRACT

Based on the Affine transformation and Partitioning techniques, we present here an adaptive element Subdivision Method (APSM) for efficient evaluation of nearly singular integrals. Adaptive subdivision techniques can deal with the common situation where the size and shape of boundary elements are significantly different. We first introduce the basic structure and main ideas of APSM implementation via affine transformations, then present several different kinds of element subdivision results with arbitrary shapes. There are several advantages of the APSM over other element subdivision methods, including adaptive subdivision, improved accuracy, and simplicity of implementation. By means of affine transformations and partitioning techniques, it is possible to subdivide a given element into a set of projective and refinement zones. It is more flexible and convenient to perform the successful subdivision of the projective and refinement zones, respectively. In addition, the ultimate patch generation quality can be improved by incorporating certain types of boundary serendipity patches around the source point. With the introduction of these serendipity patches, the APSM is capable of considerably greater accuracy and efficiency for systematic computation of the integration scheme. Several numerical examples have been given to verify the effectiveness, feasibility and robustness of the illustrated integration schemes.

1. Introduction

The boundary element method (BEM) is an alternative technique for linear and infinite domain problems, whereas the computational mechanics technology is superior in less computation and dimensionality reduction [1,2]. With the excellent properties of the boundary-only discretizations and the semi-analytical nature, boundary integral formulation has been growing dramatically in the academic field and engineering applications [3–6]. Although the BEM maintains distinct advantages, the integrals in the boundary integral formulation involve Kernel basis function products and can be evaluated numerically for practical problems. Due to the singularity of integrals in the discretised integral equations, there have been some difficulties in applying the BEM to solving complicated engineering problems [7].

Dealing with the singularities of the Kernel basis function is one of the difficult problems of BEM [8]. Nearly singular integral is a fundamental ingredient of the BEM, which is at the core of boundary integral formulation [9,10]. Theoretically, there is no irregularity in boundary integral terms since the integrands tend to infinity with various degrees. Computationally, the magnitude of the integrand varies dramatically when the source points are relatively close to the element boundary [11]. Due to the fact that neither classical Gaussian quadrature nor the general integration techniques are suitable for evaluating such integrals, accurate evaluation of the nearly singular integrals may present considerable difficulties [12].

The integrals in the boundary integral formulation can be characterized by the strength of the singularity, the size of the elements to be integrated, and the proximity of the source points. It is possible to occur nearly singular integrals in the following situations [13]: (1) Calculating the interior quantities near geometric boundaries; (2) For the slender and irregular geometric objects; (3) Different mesh sizes of adjoining computational elements; (4) The numerical integration scheme close to the boundary of non-linear problems. For complex geometries and thin structures, however, nearly singular integrals can still be a bottleneck in BEM.

Tremendous effort has been devoted to eliminating the difficulties

* Correspondence to.
E-mail address: guoqianjian@163.com (Q. Guo).

https://doi.org/10.1016/j.enganabound.2023.08.037
Received 3 July 2023; Received in revised form 24 August 2023; Accepted 25 August 2023
Available online 4 September 2023

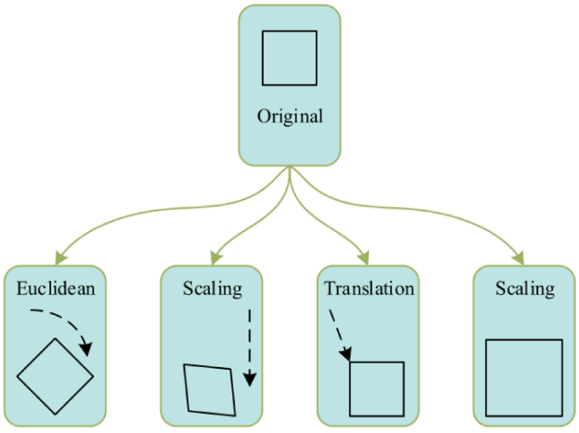

Fig. 1. The affine transformation for object representation

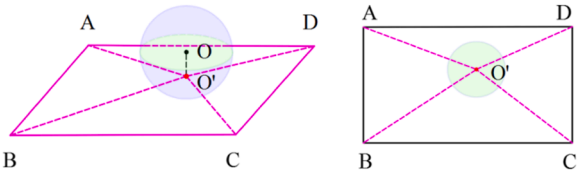

Fig. 2. The APSM procedure for evaluating nearly singular integrals

associated with nearly singular integrals, such as the adaptive subdivision strategy [14], the analytical or semi-analytical method [15], the classical Gauss quadrature method [16], and various nonlinear coordinate transformations [17–20]. Despite the success of coupling the analytical and semi-analytical method to the linear elements, there were some limitations to extending this method to solve problems involving a general distributed function and high-order elements [21]. A particular set of weights and Gaussian points is chosen in the adaptive Gaussian quadrature method [22,23], which is usually an arduous and time-consuming task for certain classes of problems. The nonlinear transformation methods are also effective in eliminating the near singularity of the integrand by transforming the Jacobi matrix. However, it is intractable to provide a common way to evaluate integrals with irregular elements [24].

With regard to the adaptive subdivision strategies, different refinement criteria determine the number of integration points required for each subregion. These subdivision techniques end up with subregions of varying size where the smaller subregions are distributed close to the nearly singular point. However, it is inevitable that the conventional element subdivision approach contains some irregular patches of inferior quality [25]. Through the hierarchical data structure of KD-tree or quad tree, the space partitioning tree method usually generates an excess of certain unnecessary subregions [26,27]. For the accurate evaluation of the integrals containing the attenuation functions with discontinuous points, the spherical refinement techniques are adopted for element subdivision based on an extensive number of empirical templates [28].

Inspired by the pioneering work mentioned above, we present an adaptive approach based on affine transformations for the evaluation of nearly singular integrals. The main feature of APSM is that it automatically takes into account the specific location of the source point. In contrast to other element subdivision methods, APSM does not need to independently construct any projective polygons for patch generation. Additionally, it is also effortless to implement the APSM for arbitrary element subdivision without any specific templates.

The remainder of the paper is outlined below. Some basic notions of adaptive element subdivision are established in Section 2, such as affine transformations for partitions, the projective zones and the refinement zones. In Section 3, we introduce the affine transformation-based refinement scheme. Several comprehensive geometry-adaptive projective zone construction techniques are presented in Section 4. In Section 5, we provide an illustration of the optimal techniques for generating ultimate patches by the serendipity patches. Several numerical examples are provided in Section 6. Section 7 summarizes and illustrates the potential of the proposed adaptive approach.

2. The affine transformation-based partition scheme

2.1. An overview of affine transformations

Based on the insight that the homography between two windows of corresponding features can be geometrically approximated by an affine transformation model, the affine transformation-based partition scheme is presented. The detailed operation process of APSM involves the following steps: element data processing, initial element partitioning, the projective and refinement zones construction, and final patch generation. By using the affine transformation-based partition scheme, the prescribed element can be subdivided into a projective zone and several refinement zones. The APSM is aimed to generate block-structured subdomains for nearly singular integrals by introducing the optimal element subdivision scheme.

As a geometric transformation, an affine transformation transforms a vector space into another vector space by a linear transformation and a translation. Any combination of linear transformations can transform a cluster of scattered points belonging to a geometric entity into another cluster. Generally, affine transformations involve rotation, scaling, shear, and translation in spatial coordinate systems (see Fig. 1). Mathematically, a series of affine transformations can be expressed by an overall transformation matrix. It can maintain the parallelism, flatness, and collinearity of the given geometric object. There is a well-established mathematical foundation for the theory of affine transformations, which has been applied extensively in a wide range of engineering applications. In the APSM implementation, the affine transformation- based subdivision scheme using the scaling and translation transformations is conducted, which is defined as follows:

$$\begin{aligned} \boldsymbol{V}^* &= \boldsymbol{V} \times \boldsymbol{D} \times \boldsymbol{S} \\ \mathbf{V}^* &= \begin{bmatrix} x \\ y \\ z \\ 1 \end{bmatrix} \begin{bmatrix} 1 & 0 & 0 & T_x \\ 0 & 1 & 0 & T_y \\ 0 & 0 & 1 & T_z \\ 0 & 0 & 0 & 1 \end{bmatrix} \begin{bmatrix} S_x & 0 & 0 & 0 \\ 0 & S_y & 0 & 0 \\ 0 & 0 & S_z & 1 \\ 0 & 0 & 0 & 1 \end{bmatrix} \end{aligned} \tag{1}$$

where **D** is the translation matrix, **S** is the scaling matrix. S_x, S_y, S_z are the scaling factors, (T_x, T_y, T_z) is the translation vector. The homogeneous coordinates of $\mathbf{V}^*$ are determined by a sequence of affine transformations for the point **V**. A detailed illustration about affine transformations are available in [29,30].

2.2. The element projective zone construction

As is illustrated in Fig. 2, the point *O* is called the source point, which is placed on the outside of the given surface element ABCD. The point labeled *O*' is called the reference singular node, and it is the nearest point on the element obtained from the source point *O*. The blue sphere is centered at the source point *O*. The green region surrounding the reference singular node *O*' is then carried out by the intersection between the sphere and the given element. Given the arbitrariness of the position of the source point with respect to the element, it is extremely difficult to construct the desired projective zone directly. Based on the remarkable properties of excellent reliability and strong stability, it is achieved using the affine transformation to divide an element into a number of block-structured subregions. In comparison with the Binary-Tree Subdivision Method (BTSM) [31], it is more flexible to construct

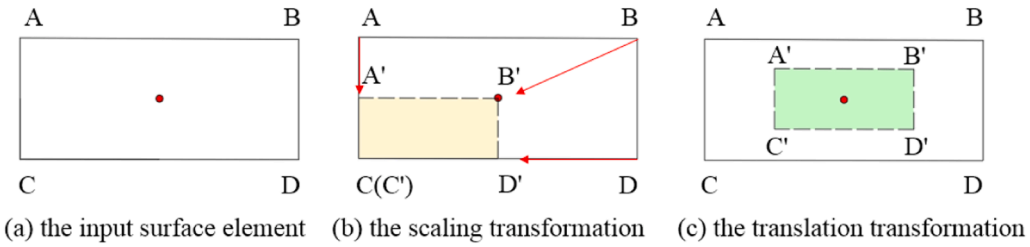

Fig. 3. Schematic of the projective zone construction

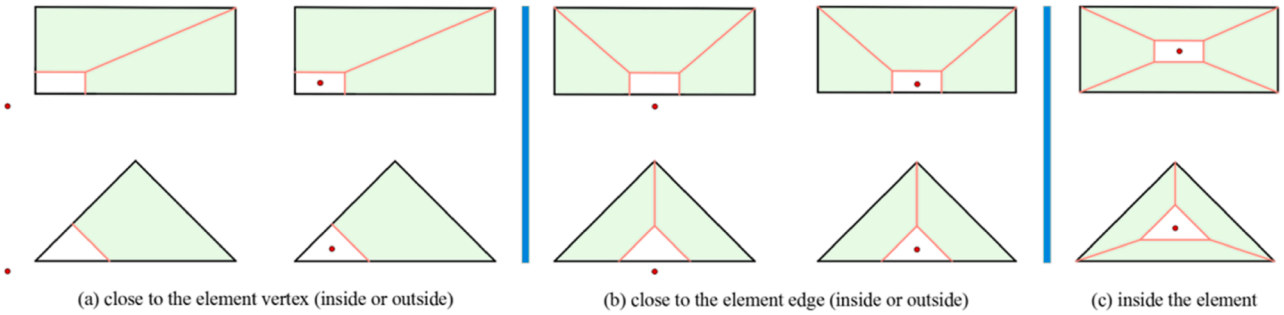

Fig. 4. Different decomposition templates for the projective zone construction

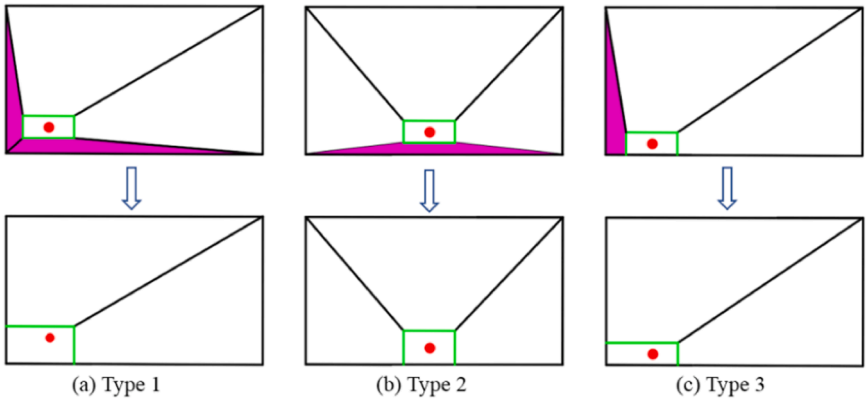

Fig. 5. The geometry-adaptive partition templates for regular elements

the projective zone by the proposed method without considering any complicated intersection problem.

A graphical representation of the projective zone construction algorithm is provided in Fig. 3 to illustrate the element partition scheme. The rectangle ABCD around the reference singular node is the boundary of the prescribed element. The elements-wise projective zones are constructed by incorporating scaling and translation transformation techniques. These streamlines of the miniaturized rectangle A'B'C'D' are then extracted from the nodes of the rectangle ABCD. It is also defined as the ratio η of the minimum distance r and the maximum distance d between the reference singular node and the element boundary. After that, the ultimate projective zone in the vicinity of the reference singular node can be obtained by the translation transformation technique.

In the preprocessing procedure of element subdivision, three categories of the projection of the source point are considered, namely, (a) close to the element vertex (inside or outside), (b) close to the element edge (inside or outside), and (c) inside the element (see Fig. 4). Provided the projection of the source point does not lie on the field element but relatively close to the element boundary, a desirable reference singular node near the element vertex/edge for element subdivision can always be obtained. These geometry-adaptive partition templates can then be employed to deal with the case of arbitrary element subdivisions.

As is shown in Fig. 4, the first two categories have two possible partition patterns, respectively. Templates 1 and 2 indicate that the reference singular node is close to the element vertex(inside or outside). Templates 3 and 4 represents that the reference singular node is close to the element edge(inside or outside). The miniaturized bounding box is then reset to the element boundary in order to construct the projective zone. As far as the third category is concerned, there is only one way to partition the elements, denoted Template 5. In the initial element preprocessing procedure, a given element is subdivided into a projective zone and several refinement zones. It should be noted that these basic decomposition templates do not affect the ultimate element subdivision result.

2.3. The refinement zone construction

2.3.1. Notations for element partition

After the projective zone is determined, another key part of the element decomposition scheme is the refinement zone construction. To conduct the adaptive element decomposition scheme, the geometrical features of the source point location and the element shape are required

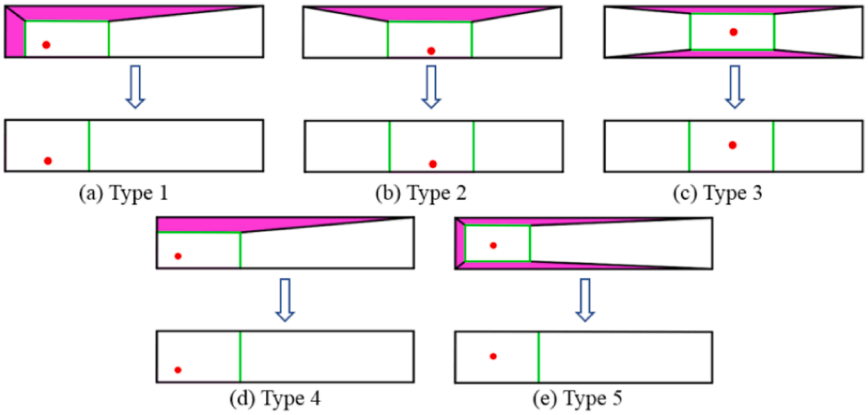

Fig. 6. The geometry-adaptive partition templates for slender elements

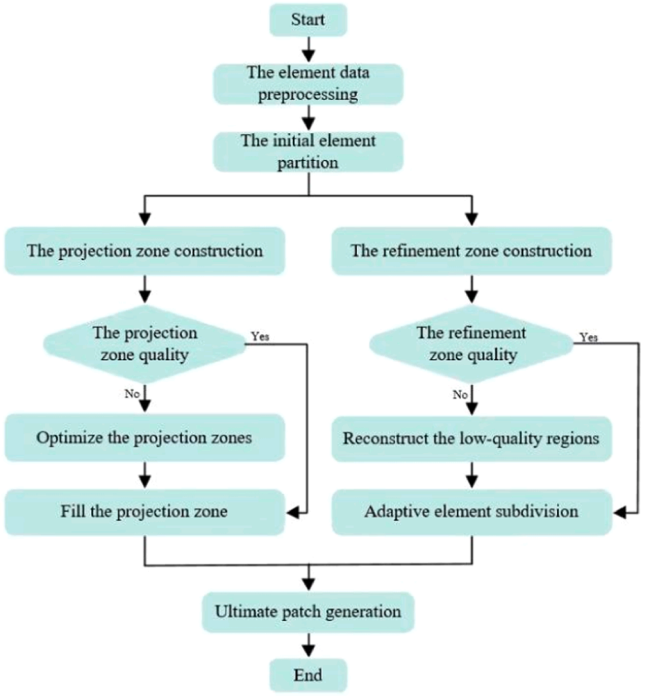

Fig. 7. Flow diagram of the affine transformations and partitioning techniques

to be recognized first. However, one of the difficulties with element features recognition is to recognize all the element decomposition templates according to the source point locations. It is still not feasible to evaluate the integrals automatically by using empirical techniques.

Aspect ratio: the ratio of the refinement zone's width to its height. Regular partition regions generally have an aspect ratio of 1.0, whereas irregular subregions often have aspect ratios of 10:1 or greater.

Reference angle: Measure the angle between adjacent segments connected with the reference singular node. The reference angle for regular triangulated subdomains is approximately 60°.

2.3.2. *Decomposition templates for geometry-adaptive partition*

As a result of the complex shapes of the elements, it is difficult to directly subdivide the prescribed elements associated with a complex geometry. To construct the refinement zones, automatic element partitioning techniques are employed to capture the geometrical features of the elements. The object element is decomposed into some geometrically adapted refinement zones based on the topological relations between the source point and the element boundaries. Several different element decomposition templates are provided for the refinement zone construction.

As depicted in Figs. 5 and 6, a detailed illustration of the element decomposition templates using the automatic partitioning scheme is presented. These basic decomposition templates for element subdivisions can be classified into three categories. Assume that the number of boundary edges of an element is N, and that the element decomposition template consists of a projective zone and at most N refinement zones. Specifically, the first category represents that the reference singular node is near the geometric edge of an element. Then, the input element is decomposed into at most N-1 refinement zones, including Type 2 in Fig. 5 and Type 2 in Fig. 6. The second category denotes that if the reference singular node is near the corner vertex, then the prescribed element is subdivided into at most N-2 refinement zones, including Type 1, Type 3 in Fig. 5 and Type 1, Type 4 in Fig. 6. The third category is where the input element is decomposed into at most N refinement zones if the reference singular node is located near the geometrical center, including Type 3, Type 5 in Fig. 6. The partitioning technique is flexible to generate reasonable initial element decomposition results for the case of arbitrary positions of the reference singular nodes.

2.3.3. *The geometry-adaptive element partition algorithm*

In the APSM implementation, the initial partition scheme should be executed to ensure the validity of the element partition. By using these geometry-adaptive partition templates, the primitive element is discretized into a set of block-structured subregions. The geometry-adaptive element partition algorithm is carried out by completing the following steps (see Fig. 7):

Step 1: Determine the position of the reference singular node and generate the initial projective zone using the affine transformation techniques.
Step 2: Construct the refinement zones by connecting the nodes of the projective zone directly to the vertices of the prescribed element.
Step 3: Evaluate the relevant partition parameters of the refinement zones, and check their validity according to the detailed criteria stated in Section 2.3.1.
Step 4: Mark the invalid refinement zones and reconstruct the ultimate element partition zones based on the basic decomposition templates in a fully automated manner.

3. Adaptive subdivision scheme for the refinement zones

3.1. *Element refinement criterion*

Similar to other spatial decomposition approaches, affine transformations were originally introduced as an important formation technique for defining geometries. Theoretically, it is also proved that affine

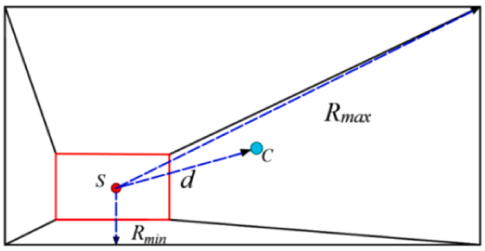

Fig. 8. Schematic of the affine transformation-based refinement criterion

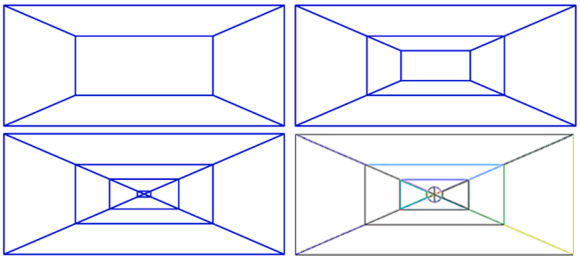

Fig. 9. The procedures of the affine transformation matching algorithm

transformations are suitable for approximating arbitrarily complicated non-manifold geometries. There are a variety of factors that influence the subdivision criteria, including element shape, kernel function, the location of source points, among others. There is a broad consensus that it is difficult to directly define a refinement function for a desirable refinement result. Instead of using the conventional element subdivision algorithm, we opt for the affine transformation scheme to subdivide elements of different types with arbitrary shapes.

The affine transformation-based refinement criterion is illustrated schematically in Fig. 8. To generate the desirable refinement subregions of the refinement zones, the affine transformation-based refinement criterion is represented as $d < R_{max}/2^i$. By definition, d represents the distance from the reference singular node and the geometric center of each sub-element. R_{min}, R_{max} denote the minimum and maximum distances from the reference singular node to the bounding rectangle, respectively. According to the refinement criterion, the primitive element node can be decomposed into a sequence of scaled leaf element nodes with similar shapes. Each of them is then checked by a refinement criterion to decide whether to proceed with the affine transformation subdivision scheme.

3.2. The affine transformation subdivision algorithm

By using the automatic partitioning techniques, the prescribed element is subdivided into several projective and refinement zones, respectively. It is more flexible and convenient to perform the successful subdivision of the projective and refinement zones, respectively. In general, the detailed procedure of the affine transformation subdivision scheme consists of the following steps:

Step 1: Calculate the relevant geometric parameters of d, R_{min}, R_{max} according to the ultimate element partition zones.
Step 2: Take the desirable refinement zones and perform the affine transformation scheme for patch generation.
Step 3: Reconstruct the refinement structure of the scaled leaf element nodes, if the bounding box extends far beyond the boundary of the root element node.
Step 4: Construct a rational admissible element refinement structure by merging smaller-sized sub-elements with their neighbors.
Step 5: Consider whether to proceed with the affine transformation subdivision scheme until the subdivision criterion is satisfied.

4. Boundary matching of the projective zone

4.1. The projective polygon construction

Based on the element partitioning scheme, a given element is subdivided into several block-structured projective and refinement zones. According to the basic element partition templates, reference singular nodes are not always located at the center of the projective zone. It is extremely difficult to generate well-shaped sub-elements by connecting the nodes of the projective zone with the reference singular node.

An essential requirement for successful element subdivision is that the boundary of the projective zone should be as close as possible to the reference singular node. Taking into account the void spaces inside the projective zone, it is reasonable to subdivide the element by projecting the polygons layer by layer along the specified direction. Then, boundary matching procedures can be implemented by selecting the boundaries of refinement sub-elements around the reference singular node to be components of the ultimate element polygon.

4.2. The affine transformation matching algorithm

Assuming that the reference singular node is near the center of the projective zone, the affine transformation matching algorithm is employed to match the projection polygon to the reference singular node layer by layer. In addition, considering the singularity order of the integrand, the affine transformation matching algorithm for filling the void space can be implemented by a number of sub-elements with different sizes and shapes.

As is depicted in Fig. 9, the procedure of the affine transformation matching algorithm is performed using the translation and scaling techniques. The projective zone is subdivided into a series of well-defined sub-elements with varying scale factors. The newly generated sub-elements surrounding the reference singular node are constructed by several layers of triangular and quadrilateral sub-elements. Due to its self-adaptive spatial subdivision properties, the affine transformation matching algorithm is robust and flexible to be applied in APSM implementations.

4.3. The binary-tree refinement matching algorithm

Due to the introduction of the element decomposition templates, the reference singular node is generally located on the side of the given element. In the particular case, the projective zone cannot be completely filled with the above affine transformation matching procedure. Based on the adaptive binary-tree refinement matching algorithm, the well-formed refined structures are generated to capture the features of the projective zone. Although the initial projective zone construction may be undesirable for the reference singular node, the ultimate well-shaped patches in the vicinity of the reference singular node can be obtained by the affine transformation matching algorithm and the binary-tree subdivision matching algorithm.

As is illustrated in Fig. 10, the projective zone is initially divided into two subregions, each of which is compared to the refinement criteria to determine whether the refinement matching scheme should proceed. To avoid unnecessary and ineffective iterations, there is also a specified minimum distance between the center of each subregion and the reference singular node. Depending on the position of the reference node and the order of the singularity, the maximum number of iterations in the binary-tree subdivision matching procedure is in the range 3 to 6. Based on the flexible configuration properties of the BTSM, the projective zone can be well decomposed by the binary-tree subdivision matching algorithm.

4.4. The curved boundary matching algorithm

In order to create well-shaped patches adjacent to the reference

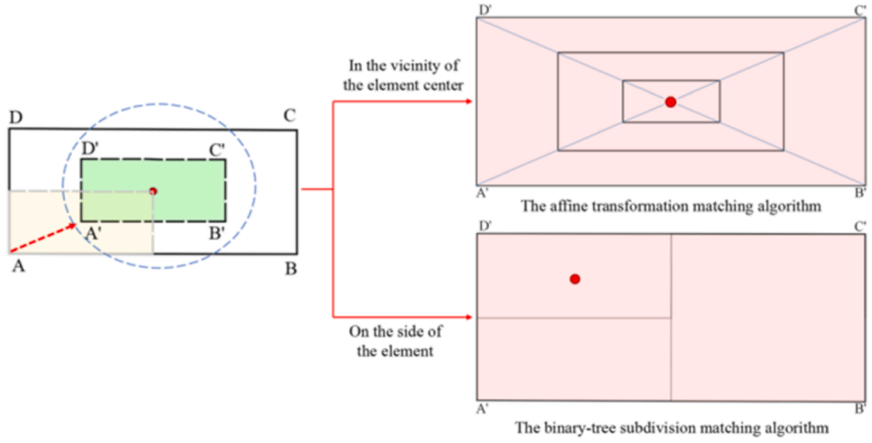

Fig. 10. Adaptive subdivision of the projective zone

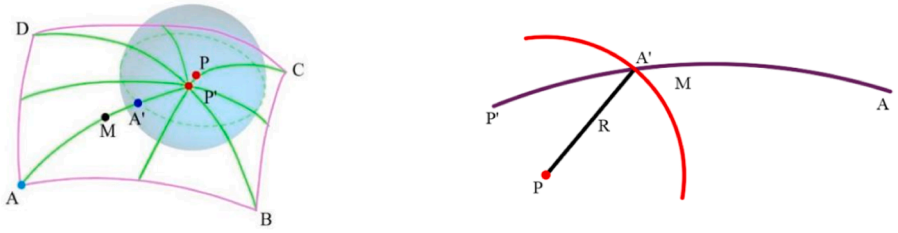

Fig. 11. The curved boundary matching procedure

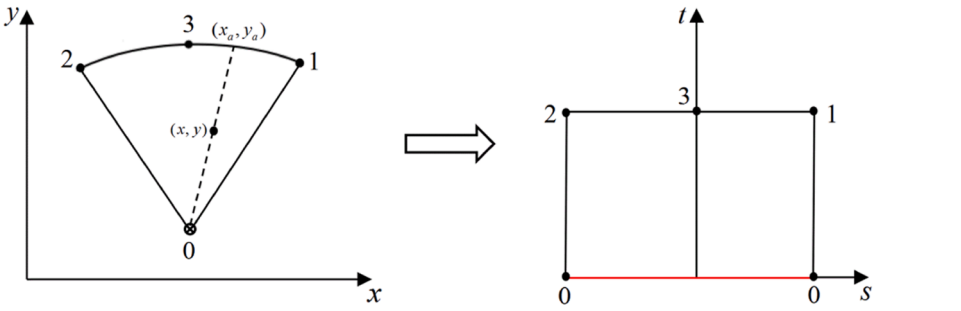

Fig. 12. Schematic of the triangular serendipity patch

singular nodes, curved boundary serendipity patches are used to evaluate nearly singular integrals. For adaptive element subdivision of higher-order elements, the greatest challenge is to accurately match the nodes of the projective zone to the sphere centered at the source point. The boundary matching algorithm using Newton iterations has been demonstrated for curved boundary elements. Compared with other matching procedures, the proposed technique has the advantages of robustness, feasibility, and fewer iterations.

A schematic description of the curved boundary matching algorithm with Newton iterations is illustrated graphically in Fig. 11. Consider an arbitrary curved boundary quadrilateral element *ABCD*, the source point*P*is close to the curved boundary surface. In essence, the problem involves obtaining target projective points on the spherical surface as well as the curved boundary of an element. The optimization function of the curved boundary matching algorithm is defined as

$$F(t) = |C(t) - O|^2 - R^2 \tag{2}$$

and the iterative sequence can be expressed as

$$t_{k+1} = t_k - \frac{(|C(t_k) - O| - R)|C(t_k) - O|}{(C(t_k) - O)\cdot C'(t_k)} \tag{3}$$

where $C(t)$ is a point on the curve along the specific projection direction, Rindicates the radius of the sphere, $|C(t) - O|$ represents the distance between the point $C(t)$ and the spherical center O, t_k and t_{k+1} are the parametric coordinates in steps k and $k+1$, respectively.

As is shown in Fig. 11, for an arbitrary boundary node A of the projective zone, the curved boundary matching algorithm is available

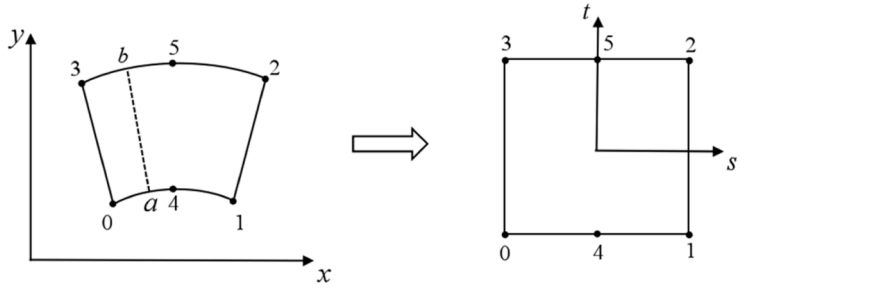

(a) a quadrilateral serendipity patch in the *x*-*y* system (b) local parametric coordinates of the patch

Fig. 13. Schematic of the quadrilateral serendipity patch

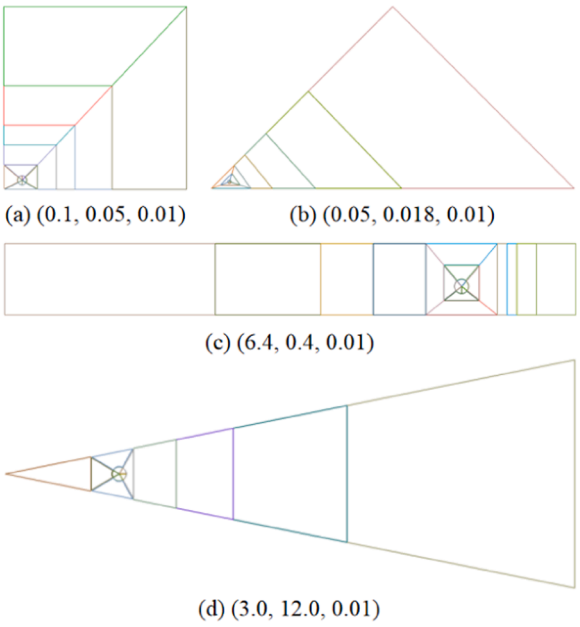

Fig. 14. The results of element subdivision for different types of elements by the APSM

for filling the void spaces based on the Newton iteration. Take the quadratic surface element for instance. Provided that the curved surface *ABCD* is the part of the given element, the crucial issue is how to match the boundary vertices to the sphere. In order to obtain the target projective node of *A*, a quadratic curve $\overset{\frown}{AMP'}$ can be generated according to the curved boundary surface. The midpoint *M* is interpolated by the reference node *P*′and the end node *A*. The optimal value of the optimization function is minimized to determine the intersection node *A*′. The intersection node *A*′ is the target projective point of an arbitrary boundary node *A*. In this way, the complicated intersection problem is transformed into the computation of the intersection of a conic with a sphere. The results demonstrate the superiority and feasibility of the curved boundary matching algorithm based on Newton iterations.

5. Patch generation around the reference singular node

The generation of patches surrounding the reference singular node is vital to the success of element subdivision. For filling the void space between the projective zone boundary and the reference singular node, several comprehensive techniques based on serendipity patches are applied. In this paper, the following boundary integral in the general form is given by

$$I(P) = \int_{\Gamma} f(P,Q)N(Q)d\Gamma = \int_{\Gamma} \frac{\bar{f}(P,Q)}{r(P,Q)} N(Q)d\Gamma \tag{4}$$

where $f(P, Q)$ is the integral kernel function, $\bar{f}(P,Q)$ is the non-singular part of the kernel function, $N(Q)$ refers to the shape function, Γ is the region of integration, P is the source node, Q is the field node, r denotes the distance between P and Q.

5.1. The triangular serendipity patch

For the construction of the innermost triangular sub-elements, the triangular serendipity patches are generated near the singular reference point. To illustrate the patch generation scheme, a graphical illustration of the triangular serendipity patch is presented in Fig. 12. For accurate representation of the spherical surface, node 0 corresponds to the

Table 1
Convergence of various integration methods for different types of elements

Element type	The locations of the source point	The number of the integration points				Relative error			
		Dist	Sinh	Sinh+S	APSM	Dist	Sinh	Sinh+S	APSM
Regular quadrilateral element	(0.1, 0.05, 0.01)	64	64	72	66	2.24E-02	2.45E-02	2.15E-02	3.15E-04
		144	144	128	135	2.81E-03	3.77E-03	2.58E-03	1.75E-05
		400	400	392	351	2.66E-04	2.66E-04	3.46E-05	2.72E-06
Regular triangular element	(0.05, 0.018, 0.01)	108	108	96	106	2.95E-02	1.18E-02	1.15E-02	2.52E-04
		192	192	150	179	9.67E-03	9.93E-03	2.98E-03	1.53E-05
		300	300	294	297	1.05E-04	1.26E-04	3.46E-05	2.48E-07
Slender quadrilateral element	(6.4, 0.4, 0.01)	144	144	128	130	3.74E-02	2.30E-02	6.33E-02	2.36E-05
		400	400	392	378	3.65E-03	3.61E-03	1.43E-02	1.57E-06
		576	576	648	558	4.07E-04	3.97E-04	1.03E-03	2.80E-07
Slender triangular element	(3.0, 12.0, 0.01)	147	147	150	157	2.42E-02	3.20E-02	1.35E-02	3.20E-05
		300	300	294	271	2.64E-03	2.16E-03	1.45E-03	1.21E-06
		432	432	384	422	8.69E-04	8.72E-04	1.09E-04	3.59E-07

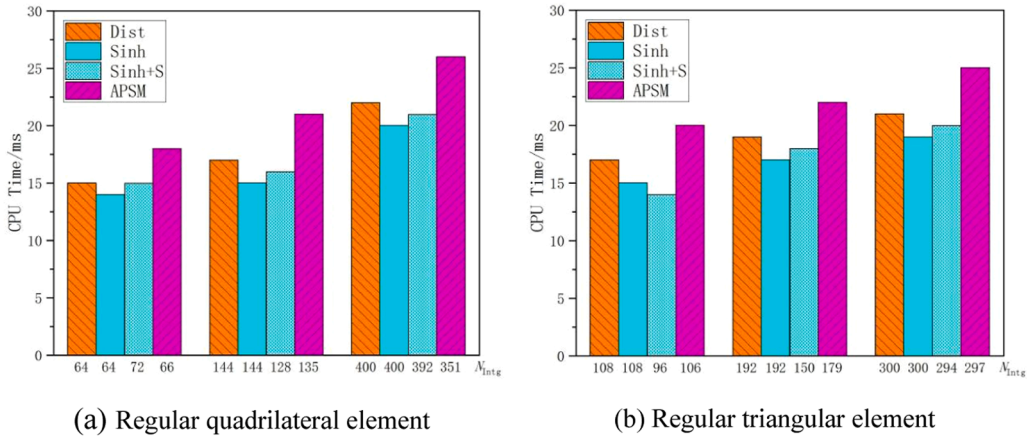

Fig. 15. Comparison of computational efficiency of different integration methods

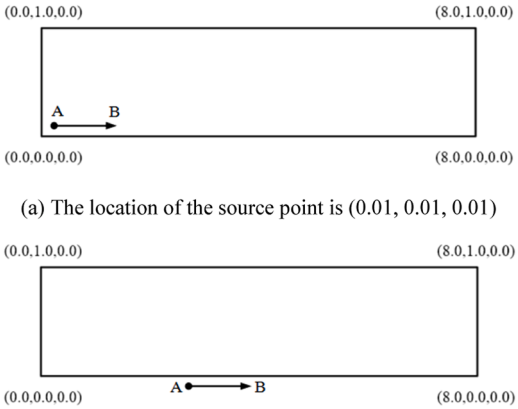

(a) The location of the source point is (0.01, 0.01, 0.01)

(b) The location of the source point is (2.70, -0.01, 0.01)

Fig. 16. The principal dimensions of the field element and the location of the source point

reference singular node, and other nodes are located along the spherical surface.

In order to evaluate the numerical integration more accurately, the coordinate transformation techniques are employed to handle the integration scheme without difficulty. Specifically, the coordinate transformation of a triangular serendipity patch in terms of nodal coordinates, which is represented as

$$\begin{cases} x_a = N_0 x_2 + N_1 x_1 + N_2 x_3 \\ y_a = N_0 y_2 + N_1 y_1 + N_2 y_3 \end{cases} \tag{5}$$

The shape functions N_0,N_1,N_2 are determined by the quadratic curve $2\,31^{\frown}$ in the local parametric coordinate system.

$$\begin{cases} N_0 = 0.5s(s-1) \\ N_1 = 0.5s(s+1) \\ N_2 = (1+s)(1-s) \end{cases} \quad s \in [-1, 1] \tag{6}$$

$$\begin{cases} x = x_0 + (x_a - x_0)t \\ y = y_0 + (y_a - y_0)t \end{cases} t \in [0, 1] \tag{7}$$

where (x_0,y_0) is the nodal coordinate of the reference singular node 0.

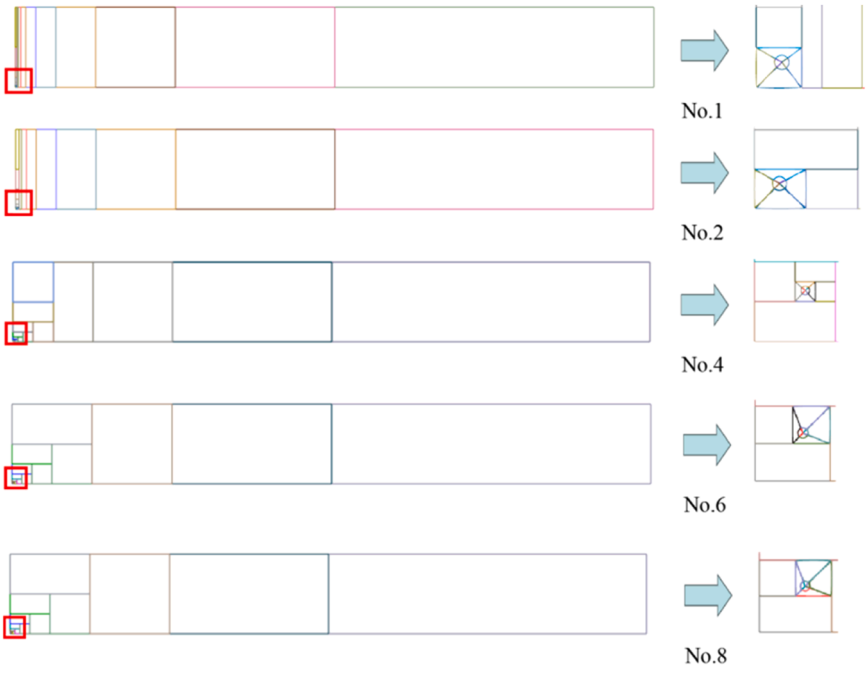

Fig. 17. The results of element subdivision for the slender quadrilateral element by the APSM

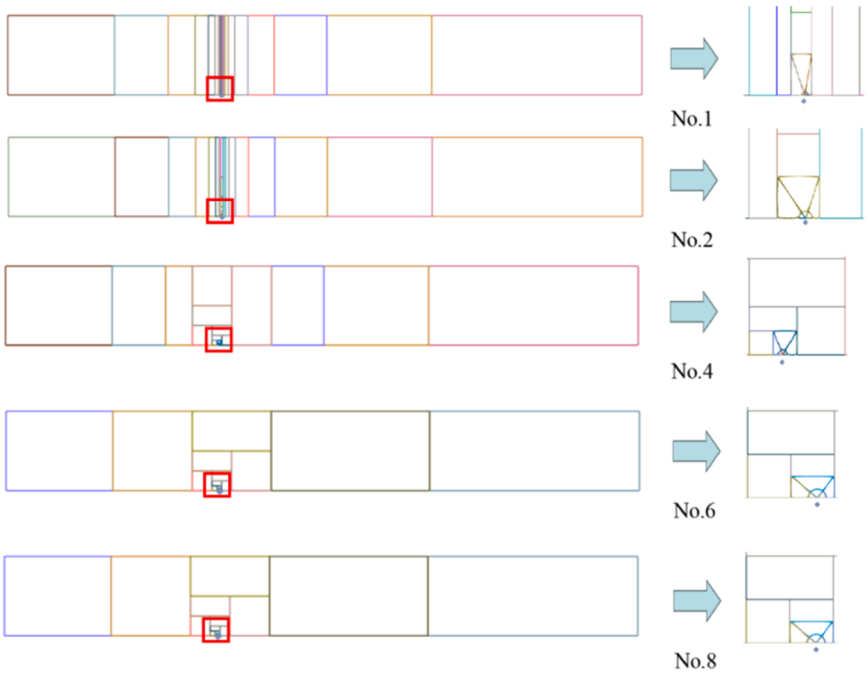

Fig. 18. The results of element subdivision for the slender quadrilateral element by the APSM

Table 2
The influence of the area of the obtained projective zone on the accuracy of the APSM

Element type	The location of the source point	Distance AB	The number of the integration points	Relative error
Slender quadrilateral element	(0.01, 0.01, 0.01)	0.01	886	5.30e-07
		0.05	651	2.82e-06
		0.1	541	7.67e-06
		1.0	438	1.37e-05
		2.0	438	1.37e-05
		3.0	432	1.43e-05
		4.0	432	1.43e-05
		5.0	432	1.43e-05

Table 3
The influence of the area of the obtained projective zone on the accuracy of the APSM

Element type	The location of the source point	Distance AB	The number of the integration points	Relative error
Slender quadrilateral element	(2.70, -0.01, 0.01)	0.01	806	1.72e-06
		0.05	628	2.18e-06
		0.1	597	3.62e-06
		1.0	398	1.51e-05
		2.0	381	2.21e-05
		3.0	374	3.57e-05
		4.0	374	3.57e-05
		5.0	374	3.57e-05

Combining Eqs. (5), (6) and (7), each point in the triangular serendipity patch can be described as

$$\begin{cases} x = x_0 + [(N_0x_2 + N_1x_1 + N_2x_3) - x_0]t \\ y = y_0 + [(N_0y_2 + N_1y_1 + N_2y_3) - y_0]t \end{cases} \tag{8}$$

Consequently, the integral of these patches in the general form can be expressed as

$$I(P) = \int_{-1}^{1}\int_{0}^{1} \frac{\bar{f}(P,Q)}{r(P,Q)} N(Q) Jb(s,t) dsdt \tag{9}$$

where

$$Jb = t\left[(x_a - x_0)\frac{\partial y_a}{\partial s} - (y_a - y_0)\frac{\partial x_a}{\partial s}\right] \tag{10}$$

5.2. The quadrilateral serendipity patch

For quadrilateral sub-elements outside the sphere, the quadrilateral serendipity patches are adopted to evaluate the integrals of these sub-elements. A graphical representation of the quadrilateral serendipity patches is shown in Fig. 13. The nodes of this type of serendipity patches are arranged in an anticlockwise direction. In geometry, the conic $0\,4\,1^{\frown}$ is formed by the intersection of the curved element with the sphere. These side edges 03 and 12 are both parallel with the diameter of the sphere. Additionally, we adopt coordinate transformation techniques to evaluate the integrals of these patches, which can be expressed as

$$\begin{cases} x = \frac{1}{2}(1-t)x_a + \frac{1}{2}(1+t)x_b \\ y = \frac{1}{2}(1-t)y_a + \frac{1}{2}(1+t)y_b \end{cases} \tag{11}$$

where the points (x_a,y_a),(x_b,y_b) are distributed along the quadratic curves $0\,4\,1^{\frown}$ and $3\,5\,2^{\frown}$, respectively.

$$\begin{cases} x_a = N_0x_0 + N_1x_1 + N_2x_4 \\ y_a = N_0y_0 + N_1y_1 + N_2y_4 \end{cases} \tag{12}$$

$$\begin{cases} x_b = N_0x_3 + N_1x_2 + N_2x_5 \\ y_b = N_0y_3 + N_1y_2 + N_2y_5 \end{cases} \tag{13}$$

where N_0, N_1, N_2 of Eqs. (12) and (13) are given by

$$\begin{cases} N_0 = 0.5s(s-1) \\ N_1 = 0.5s(s+1) \quad s \in [-1,1] \\ N_2 = (1+s)(1-s) \end{cases} \tag{14}$$

Subsequently, each point in the quadrilateral serendipity patch can

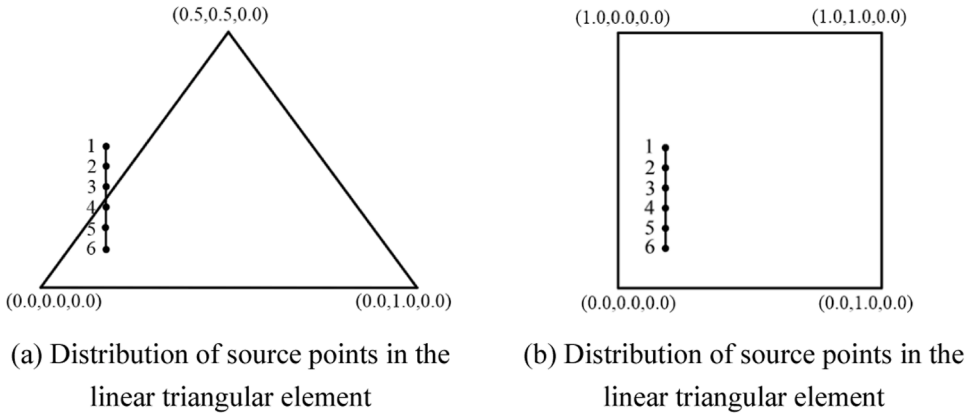

Fig. 19. Coordinates of source points and vertices of the linear elements

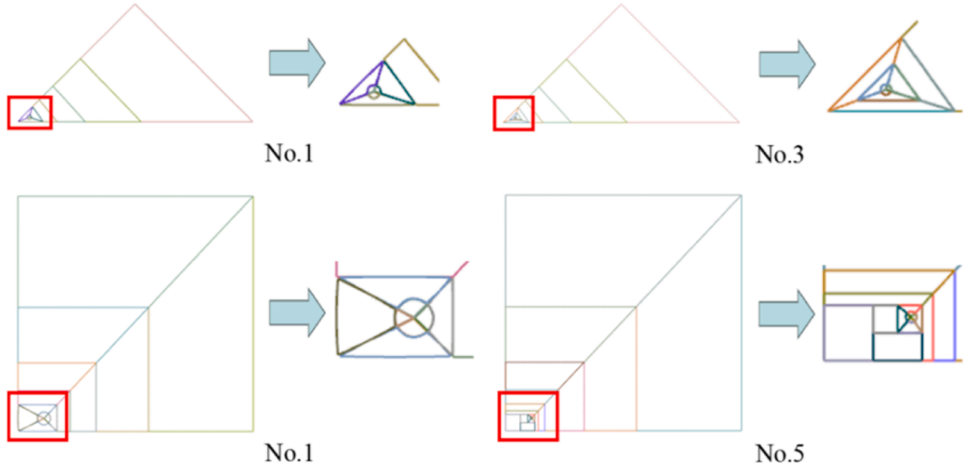

Fig. 20. The results of element subdivision for the linear surface elements by the APSM

Table 4
The integral results of various integration methods for the linear triangular element

Element type	The locations of the source point	The number of the integration points				Relative error			
		Dist	Sinh	Sinh+S	APSM	Dist	Sinh	Sinh+S	APSM
Linear triangular element	(0.05, 0.018, 0.1)	75	75	96	71	2.25e-03	1.37e-03	1.29e-03	1.59e-04
	(0.05, 0.018, 0.05)	108	108	96	101	3.80e-03	4.15e-03	1.13e-03	6.29e-04
	(0.05, 0.018, 0.01)	243	243	216	220	5.62e-04	2.45e-04	1.27e-04	7.25e-05
	(0.05, 0.018, 0.001)	363	363	294	337	6.28e-04	4.79e-04	2.46e-05	1.02e-05
	(0.05, 0.018, 0.0001)	432	432	384	397	7.58e-04	7.23e-04	1.82e-05	4.18e-05
	(0.05, 0.018, 0.00001)	675	675	600	626	3.43e-04	6.41e-04	5.51e-05	6.36e-05

Table 5
The integral results of various integration methods for the linear quadrilateral element

Element type	The locations of the source point	The number of the integration points				Relative error			
		Dist	Sinh	Sinh+S	APSM	Dist	Sinh	Sinh+S	APSM
Linear quadril-ateral element	(0.1, 0.1,0.1)	100	100	128	94	4.24e-03	4.21e-03	1.13e-04	5.59e-05
	(0.1, 0.1, 0.05)	100	100	128	116	3.86e-03	3.84e-03	2.26e-04	1.07e-05
	(0.1, 0.1, 0.01)	100	100	128	114	3.54e-03	3.57e-03	3.09e-04	2.65e-05
	(0.1, 0.1, 0.001)	324	324	288	312	1.08e-04	1.07e-04	5.46e-05	1.46e-05
	(0.1, 0.1, 0.0001)	400	400	392	418	4.54e-05	4.54e-05	1.69e-05	1.90e-05
	(0.1, 0.1, 0.00001)	576	576	648	578	1.54e-05	1.54e-05	7.61e-06	1.45e-06

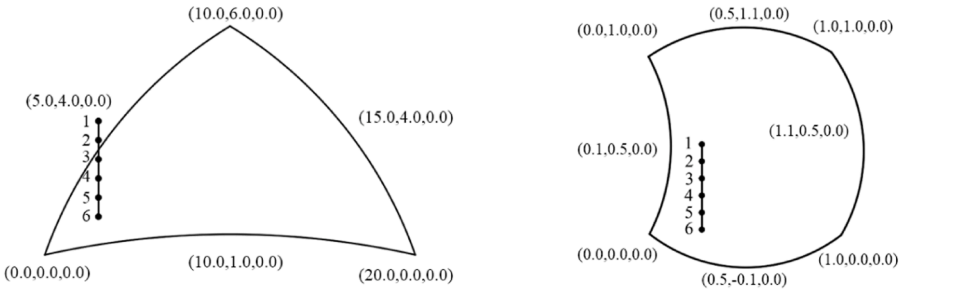

(a) Distribution of source points in the quadratic triangular element

(b) Distribution of source points in the quadratic quadrilateral element

Fig. 21. Coordinates of source points and vertices of the quadratic elements

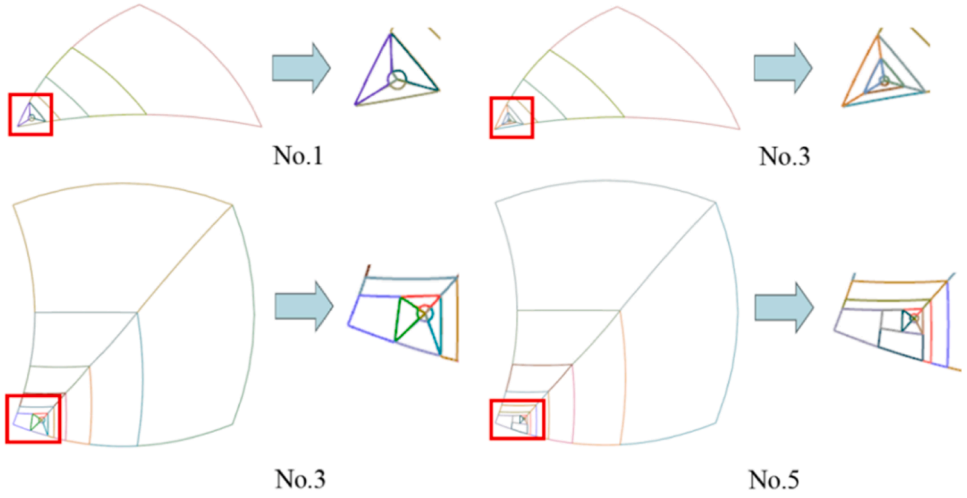

Fig. 22. The results of element subdivision for the quadratic surface elements by the APSM

Table 6
The integral results of various integration methods for the quadratic triangular element

Element type	No. of source point	The number of the integration points				Relative error			
		Dist	Sinh	Sinh+S	APSM	Dist	Sinh	Sinh+S	APSM
Quadratic triangular element	1	147	147	150	142	3.80e-03	4.15e-03	1.13e-04	2.37e-05
	2	192	192	216	202	4.63e-04	6.23e-04	3.27e-04	2.75e-05
	3	243	243	216	225	5.86e-04	5.18e-04	5.69e-04	1.28e-05
	4	300	300	294	298	7.38e-04	7.13e-04	1.82e-04	3.25e-05
	5	432	432	384	416	4.80e-04	4.74e-04	2.45e-04	2.67e-05
	6	675	675	600	628	1.38e-04	1.38e-04	6.21e-05	3.52e-06

Table 7
The integral results of various integration methods for the quadratic quadrilateral element

Element type	No. of source point	The number of the integration points				Relative error			
		Dist	Sinh	Sinh+S	APSM	Dist	Sinh	Sinh+S	APSM
Quadratic quadrilat-eral element	1	144	144	128	133	2.75e-03	2.71e-03	1.93e-03	1.47e-05
	2	324	324	288	220	2.19e-03	1.78e-03	7.25e-03	2.69e-04
	3	400	400	392	350	1.69e-03	1.55e-03	3.69e-04	1.09e-05
	4	400	400	392	398	1.12e-04	1.08e-04	7.45e-04	3.11e-05
	5	576	576	512	510	6.26e-04	6.17e-04	1.36e-05	2.08e-06
	6	676	676	648	660	2.62e-04	2.62e-04	6.33e-05	4.81e-07

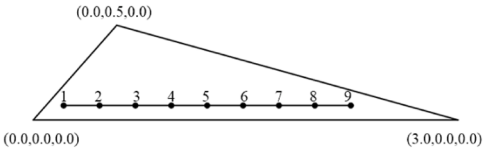

Fig. 23. Coordinates of source points and vertices of the slender triangular element

be described as

$$\begin{cases} x = \sum_{i=0}^{5} L_i x_i \\ y = \sum_{i=0}^{5} L_i y_i \end{cases} \tag{15}$$

where

$$L_0 = -0.25s(1-s)(1-t) L_1 = 0.25s(1+s)(1-t) L_2 = 0.25s(1+s)(1+t)$$
$$L_3 = -0.25s(1-s)(1+t) L_4 = 0.5\left(1-s^2\right)(1-t) L_5 = 0.5\left(1-s^2\right)(1+t) \tag{16}$$

Consequently, the integral of these patches in the general form can be rewritten as

$$I(P) = \int_{-1}^{1}\int_{-1}^{1} \frac{\bar{f}(P,Q)}{r(P,Q)} N(Q) Jb(s,t) ds dt \tag{17}$$

where

$$Jb = \begin{vmatrix} \frac{\partial x}{\partial s} & \frac{\partial y}{\partial s} \\ \frac{\partial x}{\partial t} & \frac{\partial y}{\partial t} \end{vmatrix} \tag{18}$$

By arrangement of nodes along the surface of the sphere, the kernel functions can be preferablycharacterized by the above-mentioned serendipity patches. The desirable patch generation in the vicinity of the reference singular node can be obtained by introducing the

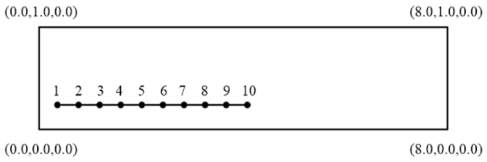

Fig. 25. Coordinates of source points and vertices of the slender quadrilateral element

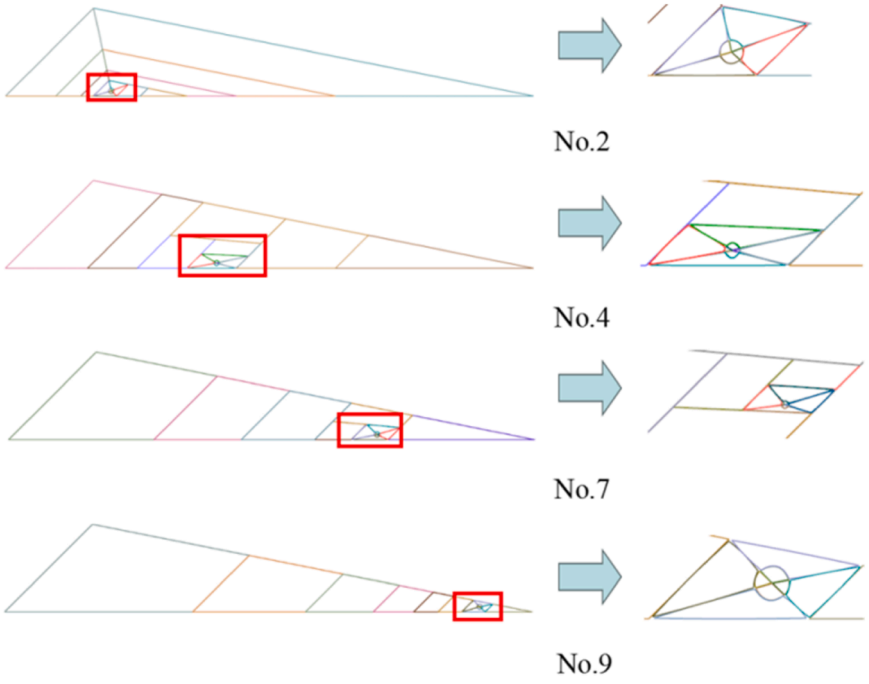

Fig. 24. The element subdivision results for the slender triangular element by the APSM

Table 8
The integral results of various integration methods for the linear triangular element

Element type	No. of source point	The number of the integration points				Relative error			
		Dist	Sinh	Sinh+S	APSM	Dist	Sinh	Sinh+S	APSM
Linear triangular element	1	675	675	726	650	2.30e-04	2.29e-04	6.29e-05	1.16e-07
	2	768	768	726	730	1.05e-04	1.05e-04	1.36e-04	3.59e-06
	3	768	768	726	745	4.07e-04	4.06e-04	3.19e-04	5.12e-06
	4	675	675	726	652	6.86e-04	6.85e-04	1.46e-04	1.62e-06
	5	768	768	726	731	2.86e-04	2.85e-04	1.72e-04	7.31e-06
	6	675	675	726	647	7.34e-04	7.33e-04	2.87e-04	6.31e-06
	7	675	675	726	692	5.08e-05	5.06e-05	3.07e-05	8.42e-07
	8	588	588	600	578	9.18e-04	9.16e-04	1.06e-04	3.92e-06
	9	588	588	600	596	8.69e-05	8.72e-05	1.09e-05	2.35e-07

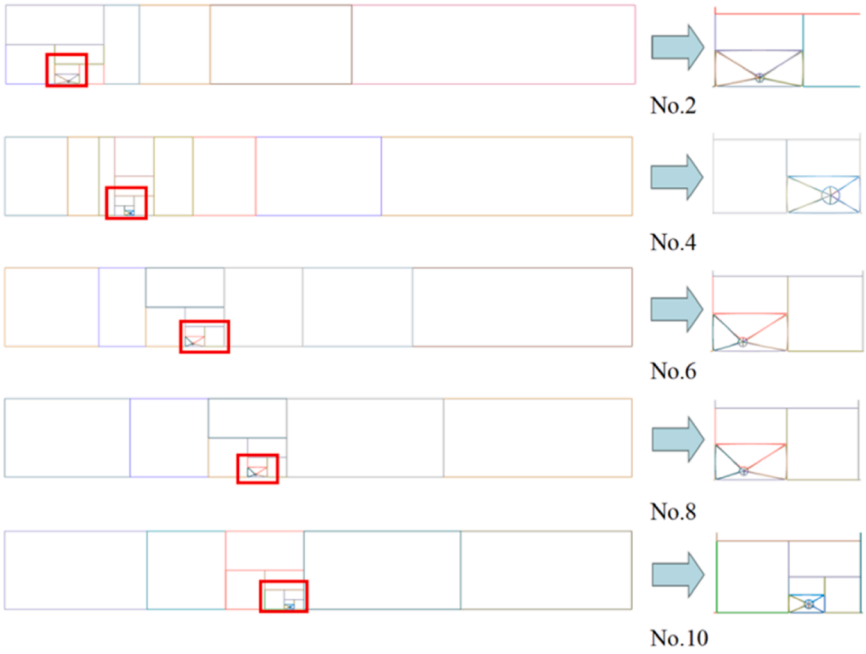

Fig. 26. The results of element subdivision for the slender quadrilateral element by the APSM

Table 9
The integral results of various integration methods for the slender quadrilateral element

Element type	No. of source point	The number of the integration points				Relative error			
		Dist	Sinh	Sinh+S	APSM	Dist	Sinh	Sinh+S	APSM
Slender quadril-ateral element	1	784	784	800	746	4.94e-04	4.89e-04	1.49e-03	5.21e-07
	2	784	784	800	728	1.04e-03	1.03e-03	6.37e-04	2.80e-07
	3	784	784	800	752	4.60e-05	4.61e-05	1.54e-03	3.91e-07
	4	784	784	800	767	4.84e-04	4.84e-04	2.21e-03	6.77e-08
	5	784	784	800	772	8.04e-04	8.04e-04	2.17e-03	7.05e-08
	6	784	784	800	786	8.50e-04	8.49e-04	3.13e-03	4.58e-08
	7	784	784	800	770	1.01e-03	1.00e-03	2.98e-03	1.58e-07
	8	784	784	800	782	1.07e-03	1.06e-03	1.53e-03	1.54e-07
	9	784	784	800	736	9.29e-04	9.29e-04	2.41e-03	4.47e-07
	10	784	784	800	762	1.13e-03	1.12e-03	3.81e-03	1.12e-07

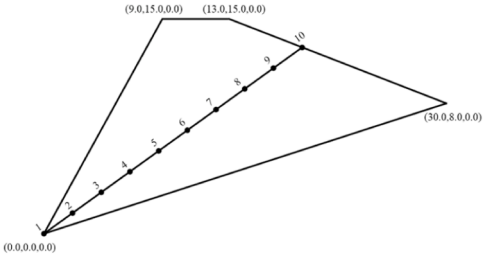

Fig. 27. Coordinates of source points and vertices of the irregular quadrilateral element

serendipity patches. Due to the excellent properties of the illustrated serendipity patches, a wide range of unnecessary quadrature points can be avoided. A detailed illustration of the triangular and quadrilateral serendipity patches can be found in [32].

6. Numerical examples

In order to demonstrate the merits of the APSM, several element subdivision examples are presented as well as comparisons with other methods. Unless otherwise mentioned, the integration methods with the notation Dist, Sinh, Sinh+S denote distance transformation, sinh transformation and sinh plus sigmoidal transformation, respectively. To verify the validity, superiority and feasibility of the APSM, we consider the following integral

$$I = \int_{\Gamma} \frac{1}{4\pi r} N d\Gamma \tag{19}$$

It is necessary to define the relative error in order to verify the calculation accuracy of APSM and other integration methods, which is given by

$$I_{err} = \left| \frac{I_n - I_e}{I_e} \right| \tag{20}$$

where N denotes the shape function of an element, I_{err} indicates the relative error of the integration scheme, I_{e} and I_{n} represent the exact and numerical values of the integral, respectively. The exact value of the integral is calculated numerically by dividing the prescribed element and increasing the number of quadrature points until the computational result is within a specified tolerance.

6.1. Accuracy and convergence performance of the APSM

6.1.1. Convergence performance of different elements subdivision

To investigate the accuracy and convergence performance of APSM,

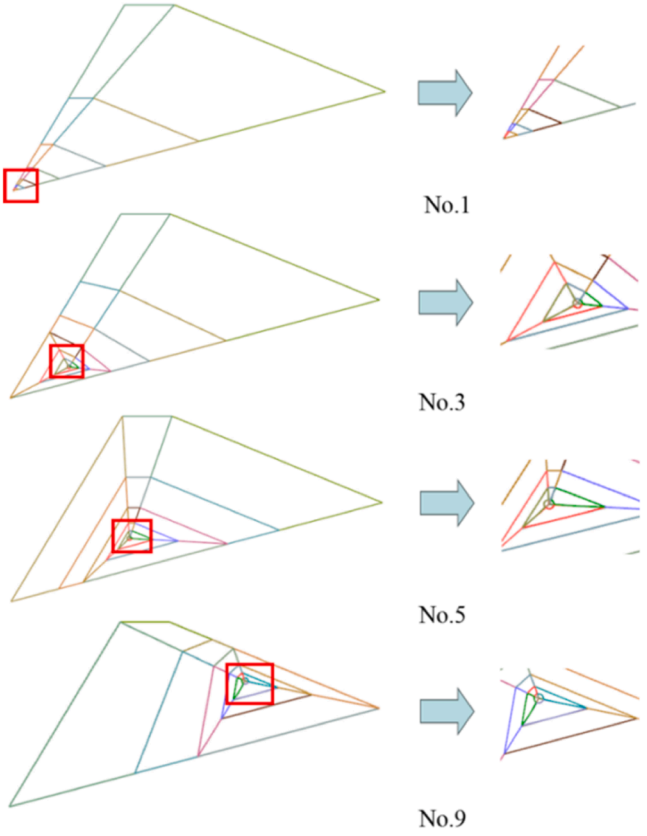

Fig. 28. The results of element subdivision for the irregular quadrilateral element by the APSM

the first group of examples are provided to confirm the astringency of the proposed method. The results of element subdivision for triangular and quadrilateral elements of different shapes and sizes are presented in Fig. 14. The integration results obtained using the Dist, Sinh, Sinh+S and APSM are provided in Table 1 for a fair comparison. A comparison of the computation times (CPU-times) of the Dist, Sinh, Sinh+S and APSM with totally 1000 calculations is provided in Fig. 15.

6.1.2. Convergence assessment on the projective zone construction

To investigate the influence of the area of the obtained projective zone on the accuracy of the APSM, a second group of examples is presented to demonstrate the accuracy and robustness of the proposed method. The principal dimensions of the field element and the locations of the source point are illustrated in Fig. 16. AB is the distance between the source point and the right boundary of the projective zone, indicating the projective zones obtained with different scale factors. The results of element subdivision for the slender quadrilateral element with different scale factors are presented in Fig. 17 and Fig. 18. The integration results obtained by the APSM are provided in Table 2 and Table 3.

As is shown in Fig. 17 and Fig. 18, the ultimate projective zones are obtained with different scale factors. Although the projection of the source point is not in the vicinity of the geometric center, the binary-tree subdivision matching algorithm is satisfactorily capable of handling this case. When the area of the projective zone is equal to the field element area, the ultimate element subdivision is then completely converted into the binary-tree subdivision algorithm. As has been demonstrated numerically in Ref. [26], the BTSM exhibits higher accuracy and more superior convergence than the conventional element subdivision

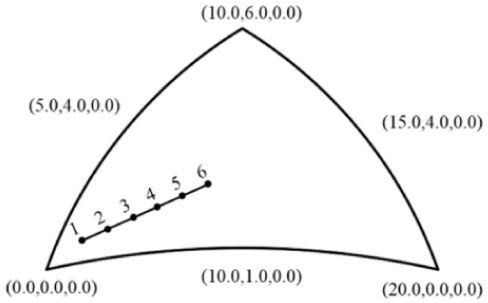

Fig. 29. Coordinates of source points and vertices of the quadratic triangular element

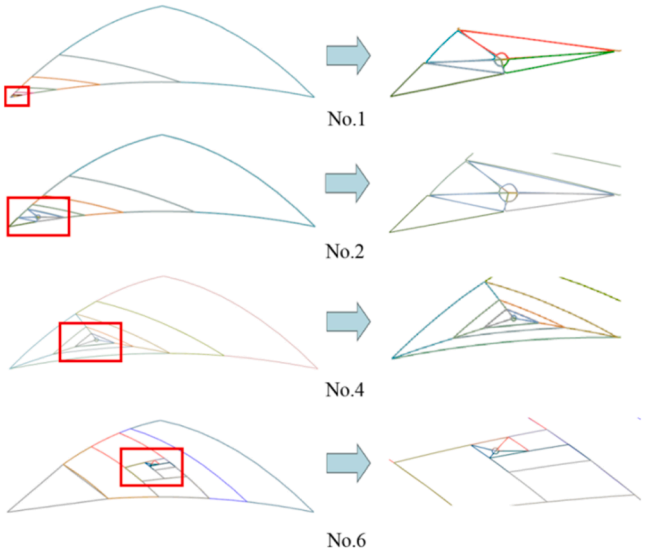

Fig. 30. The results of element subdivision for the quadratic triangular element by the APSM

Table 10
The integral results of various integration methods for a irregular quadrilateral element

Element type	No. of source point	The number of the integration points				Relative error			
		Dist	Sinh	Sinh+S	APSM	Dist	Sinh	Sinh+S	APSM
Irregular quadrilat-eral element	1	288	288	324	300	4.23e-04	1.71e-05	1.45e-05	6.07e-06
	2	324	324	288	291	1.79e-04	1.61e-04	3.19e-04	4.81e-05
	3	256	256	288	250	1.22e-04	9.26e-05	2.11e-04	1.87e-05
	4	324	324	288	283	1.27e-04	7.90e-05	5.45e-04	1.63e-05
	5	484	484	512	486	1.39e-04	7.74e-05	6.42e-04	1.81e-05
	6	484	484	512	479	8.45e-06	7.54e-07	9.82e-05	2.73e-06
	7	484	484	512	474	9.62e-06	9.62e-06	8.74e-05	1.26e-06
	8	484	484	512	480	1.79e-07	1.01e-05	2.21e-05	2.62e-06
	9	484	484	512	468	6.28e-06	1.51e-05	2.23e-05	1.11e-06
	10	300	300	294	276	3.81e-07	1.09e-06	4.94e-05	2.39e-06

Table 11
The integral results of various integration methods for the linear triangular element

Element type	No. of source point	The number of the integration points				Relative error			
		Dist	Sinh	Sinh+S	APSM	Dist	Sinh	Sinh+S	APSM
Quadratic triangular element	1	147	147	150	153	3.80e-03	4.15e-03	1.13e-04	1.56e-06
	2	192	192	216	190	4.63e-04	6.23e-04	3.07e-05	9.76e-07
	3	243	243	216	239	5.86e-04	5.18e-04	5.79e-05	5.56e-07
	4	300	300	294	288	7.38e-05	7.13e-05	1.82e-06	5.46e-07
	5	432	432	384	397	4.80e-05	4.74e-05	2.45e-06	5.51e-07
	6	432	432	384	397	1.38e-05	1.38e-05	6.51e-06	8.68e-07

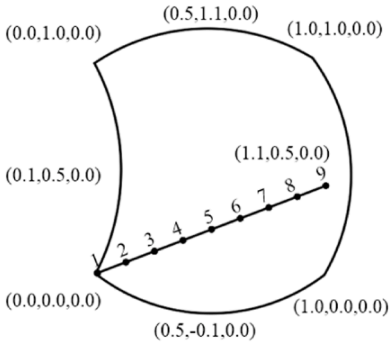

Fig. 31. Coordinates of source points and vertices of the quadratic quadrilateral element

method.

Numerical results show that the APSM has superior features, including high accuracy, stable convergence, and fast computational efficiency. The patches around the reference singular node are smaller than the distant ones. The integration points are set to be denser in the vicinity of the source point and sparsely distributed away from it. It is appealing that this processing method does not affect the ultimate element subdivision result and the integration result.

6.2. The integral results for vertical distribution of source points

6.2.1. Linear boundary surface elements

To study the performance of APSM for a smaller minimum distance from the source point to the field element, the integration results for linear triangular and quadrilateral elements are investigated. The geometry and their principal dimensions are illustrated in Fig. 19. Fig. 19 (a) plots the source points randomly distributed from (0.05,0.018,0.00001) to (0.05,0.018,0.1) in a linear triangular element. Fig. 19(b) depicts the source points randomly distributed from (0.1,0.1,0.00001) to (0.1,0.1,0.1) in a linear quadrilateral element. The results of element subdivision for linear triangular and quadrilateral elements are given in Fig. 20. Numerical results are presented in Tables 4 and 5, which demonstrate the accuracy performance of the APSM as

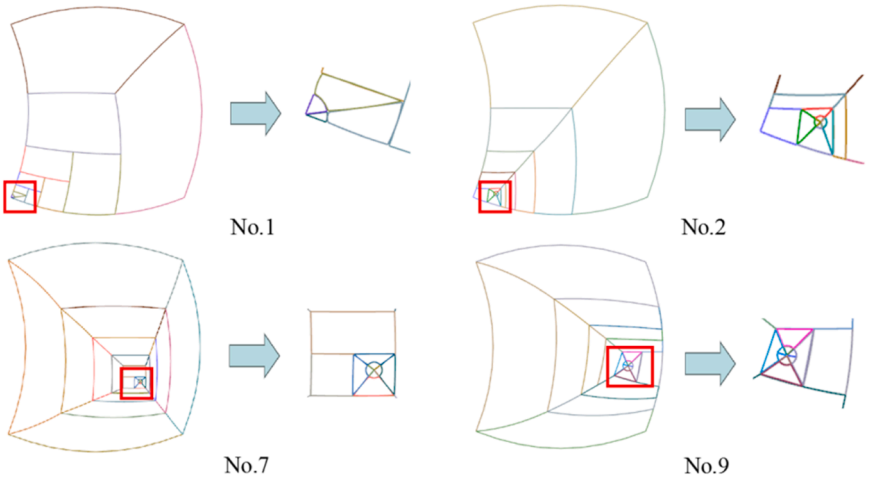

Fig. 32. The results of element subdivision for the quadratic quadrilateral element by the APSM

Table 12
The integral results of various integration methods for a quadratic quadrilateral element

Element type	No. of source point	The number of the integration points				Relative error			
		Dist	Sinh	Sinh+S	APSM	Dist	Sinh	Sinh+S	APSM
Quadratic quadrilat-eral element	1	128	128	144	138	1.09e-06	9.52e-06	6.60e-04	8.13e-06
	2	400	400	392	379	2.02e-04	2.65e-04	3.46e-05	2.73e-06
	3	400	400	392	429	3.22e-05	3.22e-05	2.01e-05	1.14e-05
	4	484	484	512	456	7.52e-07	7.90e-07	1.43e-06	9.82e-06
	5	484	484	512	493	9.95e-09	1.59e-08	6.95e-07	3.64e-08
	6	576	576	648	588	3.05e-07	4.93e-09	9.95e-09	3.74e-08
	7	484	484	512	504	8.46e-09	3.57e-09	2.93e-07	6.33e-08
	8	484	484	512	485	4.68e-08	2.24e-09	5.54e-07	3.46e-07
	9	484	484	512	468	1.49e-07	5.32e-08	5.01e-07	1.11e-07

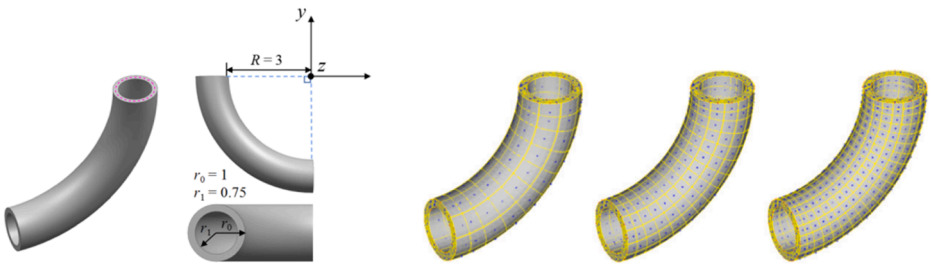

(a) Main dimensions of the elbow pipe (b) Node distribution and integration elements on an elbow pipe

Fig. 33. Geometry and mesh generation of the elbow pipe

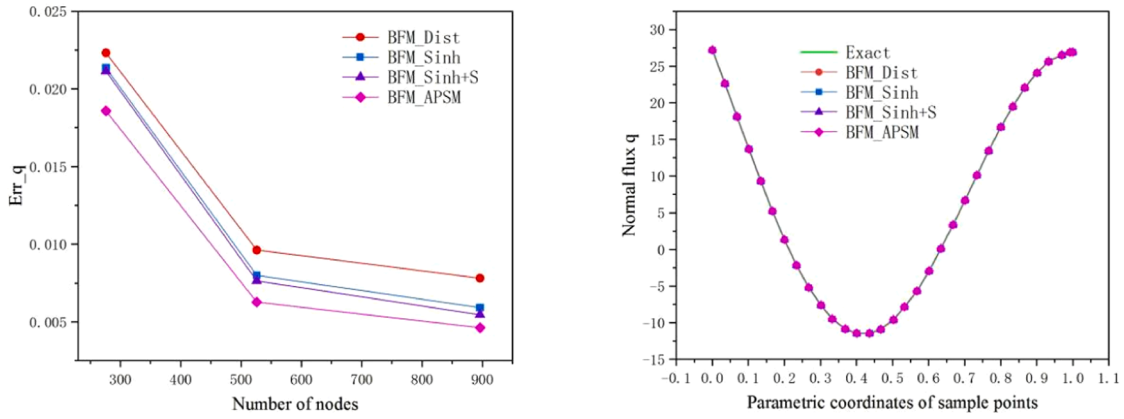

(a) The accuracy of BFM with different integration methods (b) Flux distributions along the circle curve

Fig. 34. Comparison of the accuracy of the BFM with different integration methods

compared to other conventional methods.

6.2.2. Quadratic boundary surface elements

In order to study the performance of APSM for source points at different locations, the integration results for quadratic triangular and quadrilateral elements are investigated. The main dimensions and ultimate patch generation for quadratic triangular and quadrilateral elements are shown in Figs. 21 and 22. The source points are randomly distributed from (0.1,0.1,0.01) to (0.1,0.1,0.11) in the quadratic triangular element and the quadratic quadrilateral element. Numerical results are shown in Tables 6 and 7, which demonstrate the accuracy performance of the APSM as compared to other conventional methods.

6.3. Evaluation of nearly singular integrals for irregular elements

6.3.1. Slender triangular element

The main dimensions and ultimate patch generation for a slender triangular element are shown in Figs. 23 and 24. The source points are randomly distributed from (0.3,0.03,0.01) to (2.7,0.03,0.01) in the slender triangular element. Numerical results are shown in Table 8, which demonstrate the accuracy performance of the APSM as compared to other conventional methods.

6.3.2. Slender quadrilateral element

The main dimensions and ultimate patch generation for a slender quadrilateral element are shown in Figs. 25 and 26. The source points are randomly distributed from (0.3,0.03,0.01) to (2.7,0.03,0.01) in the slender quadrilateral element. Numerical results are shown in Table 9, which demonstrate the accuracy performance of the APSM as compared to other conventional methods.

6.3.3. Irregular quadrilateral element

The main dimensions and ultimate patch generation for a irregular quadrilateral element are shown in Figs. 27 and 28. The source points are randomly distributed from (0.0,0.0,0.01) to (21.5,11.5,0.01) in the irregular quadrilateral element. Numerical results are shown in Table 10, which demonstrate the accuracy performance of the APSM as compared to other conventional methods.

6.3.4. Quadratic triangular element

The main dimensions and ultimate patch generation for a quadratic triangular element are shown in Figs. 29 and 30. The source points are randomly distributed from (0.03,0.01,0.01) to (9.4,3.1,0.01) in the quadratic triangular element. Numerical results are shown in Table 11, which demonstrate the accuracy performance of the APSM as compared to other conventional methods.

6.3.5. Quadratic quadrilateral element

The main dimensions and ultimate patch generation for a quadratic quadrilateral element are shown in Figs. 31 and 32. The source points are randomly distributed from (0.0,0.0,0.01) to (1.1,0.5,0.01) in the quadratic quadrilateral element. Numerical results are shown in Table 12, which demonstrate the accuracy performance of the APSM as compared to other conventional methods.

As depicted in Figs. 14~32, it can be concluded that the results of the ultimate element subdivision are eligible for evaluating nearly singular integrals. Based on the integration results obtained from Tables 1~12, the effective and applicable element subdivision criteria have been developed for the optimal number of quadrature points needed to yield the specified integration accuracy. The proposed algorithm overcomes the difficulty in subdividing various types of elements with arbitrary shapes under the same calculation accuracy. By combining the adaptive

subdivision strategies with affine transformations, systematic computation of the integration scheme can be performed with considerably greater efficiency.

6.4. Dirichlet problems on an elbow pipe with thin structure

To demonstrate the accuracy, feasibility and robustness of the APSM, Dirichlet problems on an elbow pipe are investigated. Since the elbow pipe is a real-world geometry with thin structure, nearly singular integrals arises in the boundary integral formulation, which have been evaluated using the proposed integration scheme. This problem is analyzed by the Boundary Face Method (BFM) [33,34] based on different integration methods with the notation BFM_Dist, BFM_Sinh, BFM_Sinh+S and BFM_APSM, respectively. For a fair comparison, the optimal number of quadrature points for each element based on the APSM should be firstly counted according to the self-adaptive subdivision criterion. Then, boundary integral formulations based on other integration methods with a similar number of integration points are implemented. In order to assess the accuracy of the BFM with different integration methods, the following analytical field is considered

$$u = -2x^2 + y^2 + z^2 \tag{21}$$

For the purpose of error estimation and convergence study, the relative L_2-norm error is defined as follows:

$$error = \sqrt{\frac{1}{N}\sum_{i=1}^{N}\left[v_i^{(e)} - v_i^{(n)}\right]^2} \tag{22}$$

where N is the total number of sample points, and the superscripts (e) and (n) denote the exact and numerical solutions, respectively.

The geometry and main dimensions of the elbow pipe are depicted in Fig. 33(a). This problem is analyzed by the BFM with totally 276, 526 and 892 nodes, respectively. A detailed illustration of the mesh generation and integration elements are given in Fig. 33(b). Dirichlet boundary conditions according to the exact solution by Eq. (21) are specified on all faces of the elbow pipe. According to Eq. (22), relative errors of nodal values of q (denoted by Err_q) are shown in Fig. 34(a). A comparison of the accuracy of the BFM with different integration methods along the circle curve is presented in Fig. 34(b).

As illustrated in Fig. 34, the accuracy of the numerical results q obtained by the BFM with APSM is greatly improved as the number of nodes increases compared to the BFM with other integration methods. It is also observed that the numerical results for q are in good agreement with the exact solution, which further demonstrates the validity of APSM for boundary integral formulation. It is concluded that the excellent properties of APSM in terms of high accuracy and superior convergence. The APSM is flexible and convenient, and could be an important technique towards more complicate geometries.

7. Conclusions

This paper presented an effective element subdivision strategy to generate a geometry-adaptive refinement structure for evaluating nearly singular integrals. By means of affine transformations and partitioning techniques, it is possible to subdivide a prescribed element into a projective zone and several refinement zones. An investigation of the performance of the APSM for evaluating nearly singular integrals has been carried out. The desirable element subdivision results have been quantified in terms of the shape and type of the prescribed elements, the relative positions of the source points.

In addition, the affine transformation-based subdivision scheme is generally applicable to the boundary integral formulation. With the introduction of these serendipity patches, it is also can be observed that the APSM is capable of considerably greater accuracy and efficiency for systematic computation of the integration scheme. The APSM could be implemented within other boundary integral formulation codes without difficulty. Combined with optimal quadrature rules for tensor product [35–37], we plan on developing the APSM to solve three-dimensional problems with hypersingular integrals in future work.

Declaration of Competing Interest

The authors declare that they have no known competing financial interests or personal relationships that could have appeared to influence the work reported in this paper.

Data availability

Data will be made available on request.

Acknowledgements

The authors would like to express their gratitude to the National Natural Science Foundation of China (12202251, 12172201, 51805299); China Postdoctoral Science Foundation, China (2021M702024, 2022M712393); Shandong Provincial Natural Science Foundation, China (ZR2022ME122, ZR2022QA072, ZR2022ME120); Special Funds for the Central Government to Guide Local Science and Technology Development (YDZX2022003); Ministry of Education Industry-school Cooperative Education Project, China (220606517023742); China Institute Electronic Labor Industry-school Cooperative Education Project (Ciel2022044); Shandong Provincial Science Foundation for the Enterprises Innovation Ability Development (2023TSGC0965); Scientific Research Project of Shandong University of Technology, China (4041/420047, 4003/122237, 9101/2222431).

References

[1] Cheng AHD, Cheng D T. Heritage and early history of the boundary element method. Engineering Analysis with Boundary Elements 2005;29(3):268–302.
[2] Zhang J M, Chi B T, Lin W C, et al. A dual interpolation boundary face method for three-dimensional potential problems. International Journal of Heat and Mass Transfer 2019;140:62–876.
[3] Xie G Z, Zhou F L, Zhang D H, et al. A novel triangular boundary crack front element for 3D crack problems based on 8-node serendipity element. Engineering Analysis with Boundary Elements 2019;105:296–302.
[4] Yang Y, Liu Y J. Modeling of cracks in two-dimensional elastic bodies by coupling the boundary element method with peridynamics. International Journal of Solids and Structures 2021;217:74–89.
[5] Gong Y, Dong C, Qin F, et al. Hybrid nearly singular integration for three-dimensional isogeometric boundary element analysis of coatings and other thin structures. Computer Methods in Applied Mechanics and Engineering 2020;367:113099.
[6] Huang J, Zhong Q, Chen H B. Radiative energy transfer model for high frequency vibration of functionally graded beams in thermal environment. Thin-Walled Structures 2023;186:110714.
[7] Gu Y, Gao H, Chen W, et al. A general algorithm for evaluating nearly singular integrals in anisotropic three-dimensional boundary element analysis. Computer Methods in Applied Mechanics and Engineering 2016;308:483–98.
[8] Gao X W, Yang K, Wang J. An adaptive element subdivision technique for evaluation of various 2D singular boundary integrals. Engineering Analysis with Boundary Elements 2008;32(8):692–6.
[9] Zhang J M, Chi B T, Singh K M, et al. A binary-tree element subdivision method for evaluation of nearly singular domain integrals with continuous or discontinuous kernel. Journal of Computational and Applied Mathematics 2019;362(4):22–40.
[10] Sladek V, Sladek J. Non-singular boundary integral representation of stresses. Int J Numer Methods Eng 1992;33(7):1481–99.
[11] Zhang J M, Chi B T, Singh K M, et al. A binary-tree element subdivision method for evaluation of singular domain integrals with continuous or discontinuous kernel. Engineering Analysis with Boundary Elements 2020;116:14–30.
[12] Cheng C Z, Niu Z R, Recho N. Effect of non-singular stress on the brittle fracture of V-notched structure. International Journal of Fracture 2012;174:127–38.
[13] Niu Z R, Wang X X, et al. A new semi-analytical algorithm for the evaluation of the nearly singular integrals in three-dimensional boundary element methods. Computer Methods in Applied Mechanics and Engineering 2005;195:1057–74.
[14] Aliabadi M H, Martin D. Boundary element hyper-singular formulation for elastoplastic contact problems. International Journal for Numerical Methods in Engineering 2000;48(7):995–1014.

[15] Hu Z, Niu Z, Cheng C. A new semi-analytic algorithm of nearly singular integrals on higher order element in 3D potential BEM. Engineering Analysis with Boundary Elements 2016;63:30–9.
[16] Lutz E. Exact Gaussian quadrature methods for near-singular integrals in the boundary element method. Engineering Analysis with Boundary Elements 1992;9 (3):233–45.
[17] Ma H, Kamiya N. A general algorithm for the numerical evaluation of nearly singular boundary integrals of various orders for two-and three-dimensional elasticity. Computational mechanics 2002;29(4):277–88.
[18] Qu W Z, Zhang Y M, Liu C S. A new regularized boundary integral equation for three-dimensional potential gradient field. Advances in Engineering Software 2016;96:83–90.
[19] Gu Y, Chen W, Zhang C Z. The sinh transformation for evaluating nearly singular boundary element integrals over high-order geometry elements. Engineering Analysis with Boundary Elements 2013;37(2):301–8.
[20] Telles J C F. A self-adaptive co-ordinate transformation for efficient numerical evaluation of general boundary element integrals. International Journal for Numerical Methods in Engineering 1987;24(5):959–73.
[21] Karami G, Derakhshan D. An efficient method to evaluate hypersingular and supersingular integrals in boundary integral equations analysis. Engineering Analysis with Boundary Elements 1999;23(4):317–26.
[22] Guiggiani M, Krishnasamy G, Rudolphi T J, et al. A general algorithm for the numerical solution of hypersingular boundary integral equations. Journal of Applied Mechanics 1992;59(3):604–14.
[23] Guiggiani M, Gigante A. A general algorithm for multidimensional Cauchy principal value integrals in the boundary element method. J Appl Mech 1990;57 (4):906–15.
[24] Xie G Z, Zhou F L, Zhang J M, et al. New variable transformations for evaluating nearly singular integrals in 3D boundary element method. Engineering analysis with boundary elements 2013;37(9):1169–78.
[25] Klees R. Numerical calculation of weakly singular surface integrals. Journal of Geodesy 1996;70(11):781–97.
[26] Zhang J M, Ju C M, Divo E, et al. A binary-tree subdivision method for evaluation of singular integrals in 3D BEM[J]. Engineering analysis with boundary elements 2019;103:80–93.
[27] Tanaka M, Zhang J M, Matsumoto T. Boundary-type meshless solution of potential problems: comparison between singular and regular formulations in hybrid BNM transactions of JASCOME. Journal of Boundary Element Methods 2003;20:21–6.
[28] Zhang J M, Lu C, Zhang X, et al. An adaptive element subdivision method for evaluation of weakly singular integrals in 3D BEM. Engineering Analysis with Boundary Elements 2015;51:213–9.
[29] Chi B T, Jia Z, Li C, et al. An adaptive element subdivision method based on the affine transformations and partitioning techniques for evaluating the weakly singular integrals. Journal of Computational and Applied Mathematics 2024;436: 115320.
[30] Bebis G, Georgiopoulos M, da Vitoria, Lobo N, et al. Learning affine transformations. Pattern recognition 1999;32(10):1783–99.
[31] Chi B T, Guo Q J, Zhang L G, et al. An adaptive binary-tree element subdivision method for evaluation of volume integrals with continuous or discontinuous kernels. Engineering Analysis with Boundary Elements 2022;134:298–314.
[32] Zhong Y D, Zhang J M, Dong Y Q, et al. A serendipity triangular patch for evaluating weakly singular boundary integrals. Engineering Analysis with Boundary Elements 2016;69:86–92.
[33] Zhang J M, Qin X, Han X, et al. A boundary face method for potential problems in three dimensions. International Journal for Numerical Methods in Engineering 2009;80(3):320–37.
[34] Zhou F L, Zhang J M, Sheng X, et al. A dual reciprocity boundary face method for 3D non-homogeneous elasticity problems. Engineering Analysis with Boundary Elements 2012;36(9):1301–10.
[35] Aimi A, Calabrò F, Falini A, et al. Quadrature formulas based on spline quasi-interpolation for hypersingular integrals arising in IgA-SGBEM. Computer Methods in Applied Mechanics and Engineering 2020;372:113441.
[36] Barton M, Calo V M. Gauss-Galerkin quadrature rules for quadratic and cubic spline spaces and their application to isogeometric analysis. Computer-Aided Design 2017;82:57–67.
[37] Hiemstra R, Calabro F, Schillinger D, Hughes T J R. Optimal and reduced quadrature rules for tensor product and hierarchically refined splines in isogeometric analysis. Computer Methods in Applied Mechanics and Engineering 2017;316:966–1004.